# Using trajectory oscillation timing improves in-flight odometry based solely on optic flows

L. Bergantin[1] *, C. Coquet[1], A. Negre[2], T. Raharijaona[3], N. Marchand[2] and F. Ruffier[1]
[1] Aix-Marseille Université, CNRS, ISM, Marseille, 13009 Marseille, France
[2] Gipsa-Lab, CNRS, Université Grenoble Alpes, 38402 Saint-Martin-d'Hères, France
[3] Université de Lorraine, Arts et Métiers Institute of Technology, LCFC, HESAM Université, F-57070 Metz, France



ABSTRACT

Traveled distance estimation is a common problem for robotic applications taking place in unknown environments where GPS is not available. In drones, the presence of weight and computational power constraints leads to the importance of developing odometry strategies based on minimilastic equipment. In this study, we imposed upon a hexarotor to perform up-and-down oscillatory motions while flying forward to test a self-scaled scheme of a visual odometer for the first time. For the odometry, the downward translational optic flow was scaled by the current visually estimated flight height and then mathematically integrated to evaluate the total distance traveled. The self-oscillatory trajectory generated successions of contraction and expansion in the optic flow vector field, which allowed to estimate the flight height of the hexarotor by means of an Extended Kalman Filter. We present three strategies based on sensor fusion that rely on no, precise or rough prior knowledge of the optic flow variations imposed by the sinusoidal trajectory. The rough prior knowledge strategy uses solely the timing of the variations of the optic flow. Tests were performed in a flying arena, where the hexarotor followed a circular trajectory while oscillating up-and-down over about $50m$ under illuminances of $117lux$ and $1518lux$.

## 1 INTRODUCTION

Traveled distance estimation of an aerial robot in an unknown environment is a common problem for all types of applications when GPS is not available. In drones, the need to reduce the Size, Weight and Power (SWaP) of the perception equipment is often of great importance to ensure the success of the task.

Several visual odometric approaches involving the use of either optic flow [1, 2], events, images & IMU combination [3] or the sparse-snapshot method [4] have been successfully tested on flying robots. All these approaches require ground height information providing the factor scaling the visual information. This scaling factor can be determined separately using a static pressure sensor [5] or stereovision [1, 4] or is integrated in the hybrid approach [3], for example. One solution to estimate the 2D position of a drone in an unknown environment is concurrent onboard odometry and visual mapping, as well as onboard SLAM (Simultaneous Localisation and Mapping) [6, 7, 8]. A minimalistic alternative is IMU (Inertial Measurement Unit) based dead reckoning - i.e. inertial integration [9]. The dead reckoning position signal could be used by a flying robot to get close enough to detect a landmark before reaching it, giving a new known starting point.

Most of these approaches require the use of computationally intensive algorithms and a feedback from the environment (such as the detection of a beacon or the feedback from a map). A minimalistic alternative is the use of optic flow cues, such as translational optic flow and optic flow divergence. Translational optic flow has been used on flying robots to visually control landing [10], to follow uneven terrain [11] and to attempt visual odometry and localisation [12, 13] (see [14] for review).

Self-oscillations have been observed in honeybees flying forward in both longitudinal and vertical tunnels ([15] and [16], respectively). The self-oscillatory motion generates a series of expansions and contractions in the optic flow vector field: the optic flow divergence cue. Visually controlled landing was achieved by using optic flow divergence [17, 18, 19, 20]. The instabilities due to the oscillatory movement have been used to determine the flight height of a micro-flyer by exploiting the linear relation between the oscillation and the fixed control gain [19]. The instabilities due to depth variation have been used to assess the optic flow scale factor of the observed scene to perform visual odometry onboard an underwater vehicle [21]. In [22], the local optic flow divergence was measured by means of two optic flow magnitudes perceived by two optic flow sensors placed on a chariot performing back-and-forth oscillatory movements in front of a moving panorama. The local optic flow divergence was then used to estimate the local distance between the chariot and the moving panorama by means of an Extended Kalman Filter (EKF).

In this study, we investigate how to include some knowledge about the trajectory oscillations in an odometry strategy based only on optic flow cues. The optic flow based odome-

*Email address: lucia.bergantin@univ-amu.fr

try scheme, called SOFIa (**S**elf-scaled **O**ptic **F**low time-based **I**nteg**a**tion model), was tested here for the first time on a hexarotor equipped with optic flow sensors that oscillated up-and-down following a circular trajectory of about $50m$. The SOFIa model was previously assessed in bio-plausible simulations to model the visual odometer of honeybees [23]. The estimation of the distance traveled by means of the SOFIa method is based on the integration of the local translational optic flow scaled by the flight height of the drone, which is estimated by means of an EKF taking the local optic flow divergence as measurement. Such integration scheme can therefore be considered as a minimalistic dead reckoning solution based on optic flow.

First, we applied the SOFIa method using only 2 optic flow measurements perceived along the longitudinal axis of the drone, with no prior knowledge of the optic flow variations. Then, to increase the odometry accuracy, we tested a sensor fusion strategy based on the parameters of the self-oscillation using 4 optic flow sensors embedded on the hexarotor. The idea was to use some prior knowledge of the oscillations imposed upon the drone to better evaluate the optic flow divergence and the translational optic flow cues. We tested two different sensor fusions based respectively on a precise and on a rough prior knowledge of the optic flow variations. The sensor fusion based on a rough prior knowledge uses solely the timing of the variations of the optic flow. All three optic flow based odometry processing were tested on bouncing circular trajectories of about $50m$ under illuminances of $117lux$ and $1518lux$.

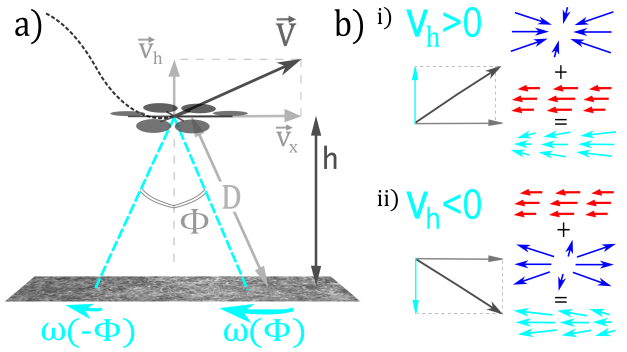


Figure 1: Hexarotor oscillating up-and-down while flying forward over the ground. a) The hexarotor's velocity $V$ can be decomposed in the components $V_x$ and $V_h$. Along the hexarotor's longitudinal axis $x$, the optic flow sensors are set at angles $\pm\phi$ with respect to the hexarotor's vertical axis and at a distance $D$ with respect to the ground. They perceive the optic flow magnitudes $\omega(\phi)$ and $\omega(-\phi)$, respectively. This configuration is found along the hexarotor's lateral axis $y$ as well. b) If $V_h$ is positive, the optic flow divergence component is a contraction (i); if it is negative, the optic flow divergence component is an expansion (ii). The contraction or expansion of the optic flow is superimposed in the ventral optic flow vector field on the translational optic flow.

In section 2, we discuss the measurement of the local translational and divergence optic flow cues. In section 3, we discuss the minimalistic visual odometer method. In section 4, we describe the hexarotor and the optic flow sensors used. In section 5, we describe the odometry processing based on the raw measurements of 2 optic flow sensors without any prior knowledge of the optic flow variations. In section 6, we describe the sensor fusion odometry processing based on 4 optic flow sensors, both with a precise and with a rough prior knowledge of optic flow variations. In section 7, we show experimentally that the sensor fusion strategies based on the knowledge of optic flow variations increase the measurement accuracy of the local optic flow cues by comparing the three methods. Finally, we compare the performance of the minimalistic in-flight optic flow based odometry of the three methods. In section 8, conclusions are drawn and future works are discussed.

## 2 MEASUREMENT OF THE LOCAL OPTIC FLOW CUES

The translational optic flow is the pattern generated on the optic flow vector field by the translational motion of a drone flying above the ground [24]. The theoretical local translational optic flow $\omega_T^{th}$ can be expressed as the ratio between the $V_x$ component of the drone's velocity and its flight height $h$ (see Figure 1):

$$\omega_T^{th} = \frac{V_x}{h} \tag{1}$$

The local translational optic flow can be measured on a hexarotor as the sum of two optic flow magnitudes $\omega(\phi)$ and $\omega(-\phi)$ perceived by two optic flow sensors oriented at angles $\pm\phi$ with respect to the hexarotor's vertical axis, divided by a known factor of $2 \cdot \cos(\phi)^2$:

$$\omega_T^{meas} = \frac{\omega(\phi) + \omega(-\phi)}{2 \cdot \cos(\phi)^2} = \frac{V_x}{h} \tag{2}$$

In the case of a hexarotor equipped with four optic flow sensors as illustrated in Figure 2.b, three translational optic flow cues can be measured as:

- the sum of the two optic flow magnitudes perceived by the two optic flow sensors set along the longitudinal axis $x$, namely $\omega_{T_1}^{meas}$,
- the sum of the two optic flow magnitudes perceived on the $x$ axis by the two optic flow sensors set along the lateral axis $y$, namely $\omega_{T_2}^{meas}$,
- the median of the four optic flow magnitudes considered, projected on the hexarotor's vertical axis by a $1/\cos(\phi)$ factor, namely $\omega_{T_3}^{meas}$.

The series of contractions and expansions generated in the optic flow vector field by up-and-down oscillatory motions is known as optic flow divergence. When a drone flies forward

while oscillating up-and-down above the ground, in the optic flow vector field the optic flow divergence is superimposed on the translational optic flow. Due to the oscillatory movement, the state vector $X = [h, V_h]^T$ is locally observable [20]. The theoretical local optic flow divergence $\omega_{div}^{th}$ can be expressed as the ratio between the $V_h$ component of the drone's velocity and $h$ (see Figure 1):

$$\omega_{div}^{th} = \frac{V_h}{h} \tag{3}$$

In [22], the authors have mathematically demonstrated that the local optic flow divergence can be measured on a micro-flyer as the subtraction between two optic flow magnitudes $\omega(\phi)$ and $\omega(-\phi)$ perceived by two optic flow sensors oriented at angles $\pm\phi$ with respect to the normal to a surface, divided by a known factor of $\sin(2\phi)$:

$$\omega_{div}^{meas} = \frac{\omega(\phi) - \omega(-\phi)}{\sin(2\phi)} = \frac{V_h}{h} \tag{4}$$

In the case of a hexarotor equipped with four optic flow sensors, two optic flow divergence cues can be measured as:

- the subtraction between the two optic flow magnitudes perceived by the two optic flow sensors set along the longitudinal axis $x$, namely $\omega_{div_x}^{meas}$,
- the subtraction between the two optic flow magnitudes perceived by the two optic flow sensors set along the lateral axis $y$, namely $\omega_{div_y}^{meas}$.

## 3 THE SOFIA VISUAL ODOMETER METHOD

In [23], the authors have assessed in simulation a model of the honeybee's visual odometer called SOFIa (**S**elf-scaled **O**ptic **F**low time-based **I**nteg**ra**tion model). The SOFIa model is based on the integration of the local translational optic flow $\omega_T$ scaled by the estimated distance with respect to the ground $\hat{h}$:

$$\hat{X}_{SOFIa} = \int \omega_T \cdot \hat{h}\, dt \tag{5}$$

In [23], $\hat{h}$ was estimated by means of an EKF taking as input the honeybee's wing stroke amplitude and as measurement the local optic flow divergence computed as the ratio between $V_h$ and $h$ (as in equation (3)). The local translational optic flow was computed as the ratio between $V_x$ and $h$ (as in equation (1)). The SOFIa model was found to be about 10 times more accurate than the raw mathematical integration of optic flow.

## 4 MATERIALS AND METHODS

The hexarotor was developed together with Hexadrone™ and equipped with four Pixart PAW3903 optic flow sensors (see Figure 2 and Table 1). The Pixart PAW3903 optic flow sensors were embedded on printed circuits to set them on the drone. The hexarotor had as onboard low-level flight controller the PX4 autopilot system [25] and used a trajectory tracking algorithm[1] to perform up-and-down oscillating circular trajectories. Based on the intrinsic attitude stability of the hexarotor, we can consider that there is no rotational component measured by the optic flow sensors. Furthermore, we consider that pitch and roll are negligible despite the circular bouncing trajectory. Thus, the downward translational optic flow can be measured along the $x$ component of the optic flow sensors. Position and orientation used in the hexarotor's control were taken from the motion-capture (MoCap) system installed in the Mediterranean Flying Arena. The flying arena was equipped with 17 motion-capture cameras covering a 6 × 8 × 6 m volume using a VICON™ system. Datasets including the optic flow measurements were recorded via the Robot Operating System (ROS) and processed with the Matlab/Simulink 2022 software.

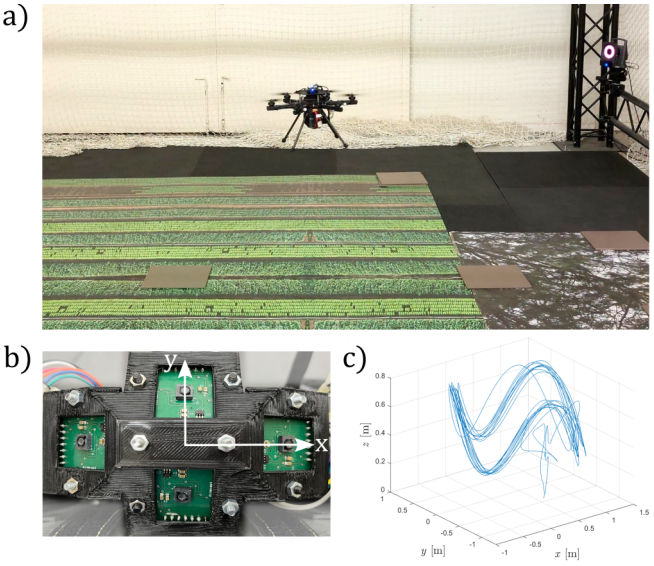


Figure 2: a) Hexarotor equipped with 4 optic flow sensors oriented towards the ground flying along a bouncing circular trajectory in the Marseille's flying arena. b) 2 optic flow sensors were set along the longitudinal axis $x$ at angles $\phi = \pm 30°$ with respect to the hexarotor's vertical axis $z$, while the other 2 optic flow sensors were set along the lateral axis $y$ at angles $\phi = \pm 30°$ with respect to the hexarotor's vertical axis $z$. c) Example of a test flight trajectory over $53m$ at an oscillation frequency of $0.28Hz$.

**State space representation used for the EKF** To estimate the hexarotor's flight height $\hat{h}$, we chose to model the hexarotor's system as a double integrator receiving as input the acceleration $a_z$ on the vertical axis $z$ given by the drone's IMU. Thus, the hexarotor's state space representation can be ex-

[1] https://github.com/gipsa-lab-uav/trajectory_control

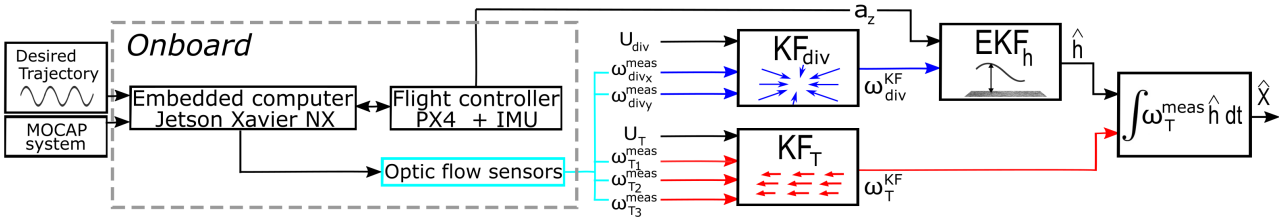


Figure 3: The sensor fusion based on 4 optic flow sensors rely on additional Kalman Filters (KF). The embedded computer handles the 4 optic flow sensors set on the hexarotor. $\omega_{div_x}^{meas}$ and $\omega_{div_y}^{meas}$ are taken as measurements by a KF (noted $KF_{div}$), that takes as input the current value $U_{div}$ of the model of the optic flow divergence. The output of the KF is the local optic flow divergence $\omega_{div}^{KF}$. $\omega_{T_1}^{meas}$, $\omega_{T_2}^{meas}$ and $\omega_{T_3}^{meas}$ are taken as measurements by a KF (noted $KF_T$), that takes as input the current value $U_T$ of the model of the translational optic flow. The output of the KF is the local translational optic flow $\omega_T^{KF}$. The EKF takes as input the hexarotor's acceleration $a_z$ and as measurement $\omega_{div}^{KF}$ to estimate the current flight height $\hat{h}$. The EKF output $\hat{h}$ scales $\omega_T^{KF}$, that is then integrated to perform odometry.

| Specifics | Optic flow sensors |
|---|---|
| Sensor chip | Pixart PAW3903 |
| Sensor PCB | 4 × 2g |
| Hardware read-out of the 4 sensors | Arduino Nano |

Table 1: Table of the specifics of the optic flow sensors equipped on the hexarotor.

pressed as:

$$\begin{cases} \dot{X} = f(X, a_z) = A \cdot X + B \cdot a_z = \begin{bmatrix} 0 & 1 \\ 0 & 0 \end{bmatrix} \cdot X + \begin{bmatrix} 0 \\ 1 \end{bmatrix} \cdot a_z \\ Y = g(X) = [X(2)/X(1)] = V_h/h = \omega_{div} \end{cases} \tag{6}$$

where $X = \begin{bmatrix} h, V_h \end{bmatrix}^T$ is the hexarotor's state vector.
The use of an EKF was necessary due to the non-linearity of the local optic flow divergence, as the measurement depends on the ratio of both states $V_h$ and $h$ (see equation (3)).

## 5 ODOMETRY METHOD WITH 2 OPTIC FLOW SENSORS WITH NO PRIOR KNOWLEDGE (NPK)

The local optic flow divergence $\omega_{div}^{2S}$ was measured as the subtraction between the two raw optic flow magnitudes perceived by the two optic flow sensors set along the $x$ axis, while the local translational optic flow $\omega_T^{2S}$ was measured as their sum. To estimate the flight height $\hat{h}$, the EKF received as:

- input: the acceleration of the drone $a_z$,
- measurement: the local optic flow divergence $\omega_{div}^{2S}$.

See Appendix B for the EKF calculations.
$\hat{h}$ was then used to scale the integration of the local translational optic flow $\omega_T^{2S}$ to perform odometry. This odometry method based on 2 raw optic flow measurements does not need prior knowledge of any parameter to assess the distance traveled.

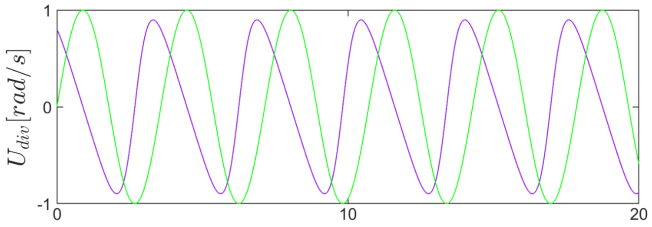


Figure 4: Inputs $U_{div}$ of the Kalman Filters (KF) used to fuse optic flow divergence cues with the **P**recise **P**rior **K**nowledge (PPK) fusion strategy (in purple) and with the **R**ough **P**rior **K**nowledge (RPK) fusion strategy (in green), respectively. In the RPK sensor fusion strategy, only a sinus helps the KF to keep the oscillation timing as the shape looks similar.

## 6 FUSION STRATEGIES WITH 4 OPTIC FLOW SENSORS

### 6.1 *Fusion strategy using a very **P**recise **P**rior **K**nowledge (PPK) of the optic flow variations*

Here, we investigated how to use prior knowledge of the self-oscillation to further improve the accuracy of the distance traveled estimates.
We expressed the optic flow divergence induced by the self-oscillation to serve as input of a Kalman Filter (KF) as follows (see Figure 4):

$$\omega_{div} = \frac{\dot{h}}{h} \longrightarrow U_{div}(k) = \frac{A_{osc} 2\pi f_{osc} \cos(2\pi f_{osc} k\delta t)}{h_0 + A_{osc} \sin(2\pi f_{osc} k\delta t)} \tag{7}$$

with $f_{osc}$ oscillation frequency equal to $0.28Hz$, $A_{osc}$ oscillation amplitude equal to $0.25m$ and $h_0$ average flight height equal to $0.55m$. To fuse $\omega_{div_x}^{meas}$ and $\omega_{div_y}^{meas}$, we used a KF (see Figure 3). At each $k^{th}$ step, the KF received as input the current value of the model in equation (7) and as measurements $\omega_{div_x}^{meas}$ and $\omega_{div_y}^{meas}$. See Appendix A for the KF calculations.

We expressed the translational optic flow induced by the

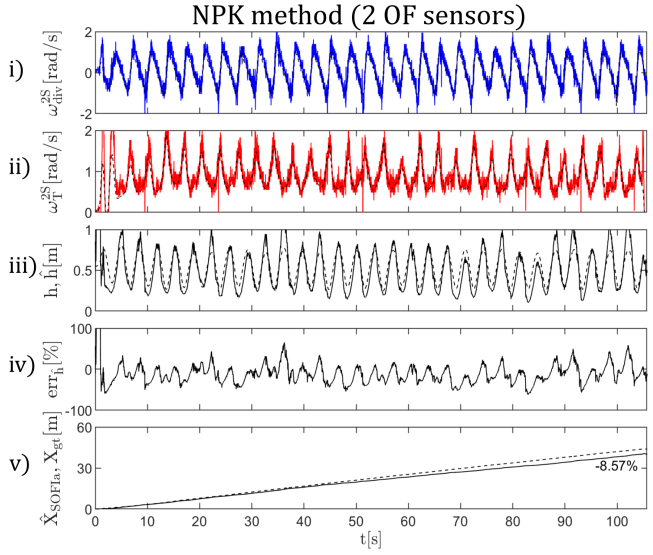


Figure 5: i) The local Optic Flow (OF) divergence $\omega_{div}^{2S}$ (in blue) measured with the **N**o **P**rior **K**nowledge (NPK) method had a Signal-to-noise Ratio (SnR) of $5.62dB$. The theoretical local optic flow divergence was computed as the ratio between $V_h$ and $h$ (in dashed line). ii) The local translational optic flow $\omega_T^{2S}$ (in red) measured with the NPK method had a SnR of $19.12dB$. The theoretical local translational optic flow was computed as the ratio between $V_x$ and $h$ (in dashed line). iii) The estimates of the flight height $\hat{h}$ converged quickly (within $4s$) to the ground truth $h$. iv) The average percentage error of $\hat{h}$ with respect to $h$ after convergence was $-9.77\%$ (with a range of $[-61.5\%, 65.34\%]$). v) The final percentage error in the estimates of the distance traveled $\hat{X}_{SOFIa}$ with respect to the ground truth $X_{gt}$ was $-8.57\%$.

forward motion to serve as input of a KF as follows:

$$\omega_T = \frac{V_x}{h} \longrightarrow U_T(k) = \frac{\omega_T^{KF}(k-1) \cdot \hat{h}(k-1)}{h_0 + A_{osc}\sin(2\pi f_{osc} k\delta t)} \quad (8)$$

$V_x(0) \approx \omega_T^{KF}(k=0) \cdot \hat{h}(k=0)$ was initialized at $0.45m/s$. To fuse the three translational optic flow cues $\omega_{T_1}^{meas}$, $\omega_{T_2}^{meas}$ and $\omega_{T_3}^{meas}$, we used a KF (see Figure 3). At each $k^{th}$ step, the KF received as input the current value of the model in equation (8) and as measurements $\omega_{T_1}^{meas}$, $\omega_{T_2}^{meas}$ and $\omega_{T_3}^{meas}$. See Appendix A for the KF calculations.

### 6.2 *Fusion strategy using a very **R**ough **P**rior **K**nowledge (RPK) of the optic flow variations*

Here, we investigated how to implement the sensor fusion strategy with 4 optic flow sensors without the knowledge of the oscillation amplitude $A_{osc}$ and the average flight height $h_0$ just by using the knowledge of the trajectory oscillation timing.
To do so, we approximated very roughly both the optic flow divergence and the translational optic flow cues to a sinusoidal signal to serve as input of both KFs as follows (see Figure 4):

$$U_{div}(k) = U_T(k) = \sin(2\pi f_{osc} k\delta t) \quad (9)$$

with $f_{osc}$ oscillation frequency equal to $0.28Hz$. At each $k^{th}$ step, both KFs received as input the current value of the model in equation (9) and as measurements the divergence optic flow measurements ($\omega_{div_x}^{meas}$ and $\omega_{div_y}^{meas}$) and the translational optic flow measurements ($\omega_{T_1}^{meas}$, $\omega_{T_2}^{meas}$ and $\omega_{T_3}^{meas}$), respectively. See Appendix A for the KF calculations.

### 6.3 *Extended Kalman Filter within the fusion strategy with four optic flow sensors*

To estimate the drone's flight height $\hat{h}$, we used an EKF that received as:

- input: the acceleration of the drone $a_z$,
- measurement: the local optic flow divergence $\omega_{div}^{KF}$ filtered by the KF based on the measurements of the optic flow sensors.

See Appendix B for the EKF calculations.
$\hat{h}$ was used to scale the local translational optic flow $\omega_T^{KF}$, that was then integrated to perform odometry as follows:

$$\hat{X}_{SOFIa} = \int \omega_T^{KF} \cdot \hat{h}\, dt \quad (10)$$

## 7 RESULTS

We compared the sensor fusion strategies based on **P**recise **P**rior **K**nowledge (PPK) and on **R**ough **P**rior **K**nowledge (RPK) of optic flow variations (using here 4 optic flow sensors) to the method based on **N**o **P**rior **K**nowledge (NPK) of optic flow variations (using here 2 optic flow sensors). 7 bouncing circular test flights of about $50m$ were performed with the hexarotor both under an illuminance of $117lux$ ($5.36 \cdot 10^{-6} W/cm^2$) and under an illuminance of $1518lux$ ($2.71 \cdot 10^{-4} W/cm^2$), for a total of 14 test flights. First, the 14 datasets were processed with the NPK method (see Section (5)). Then, the 14 datasets were processed using the PPK strategy (see Section (6.1)) and the RPK strategy (see Section (6.2)). The KF parameters defined in Appendix A were chosen as $\Phi = 10$, $\Gamma = 10$ and $H_k = 10$. The KF parameters were experimentally chosen with the first dataset taken under an illuminance of $1518lux$ and were used to process all 14 datasets for both PPK and RPK fusion strategies.
In Figures 5 and 6, the optic flow measurements were processed with the three strategies (NPK, RPK and PPK) for the same dataset taken under an illuminance of $1518lux$. The increase in the Signal-to-noise Ratio (SnR, computed as the squared ratio of the root mean square of the signal and the root mean square of its noise) observed in Figure 6 for the local optic flow divergence and the local translational optic flow between the NPK method and the PPK and RPK strategies influenced the average percentage error of the estimates

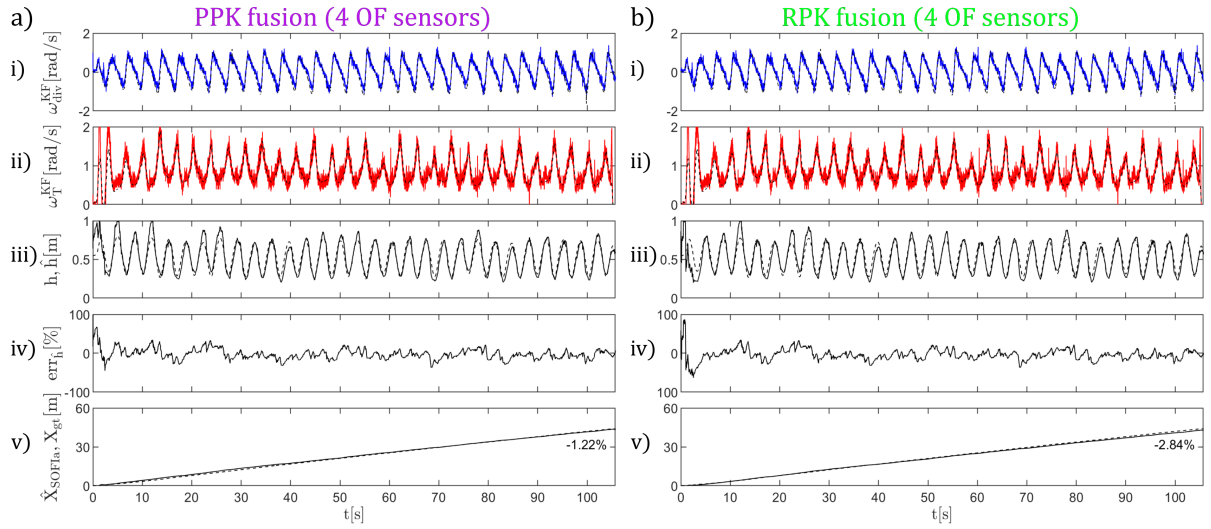


Figure 6: The local Optic Flow (OF) divergence $\omega_{div}^{KF}$ (in blue) measured with the **P**recise **P**rior **K**nowledge (PPK) strategy had a Signal-to-noise Ratio (SnR) of $6.72dB$ (a.i) and with the **R**ough **P**rior **K**nowledge (RPK) strategy of $6.73dB$ (b.i). The theoretical local optic flow divergence was computed as the ratio between $V_h$ and $h$ (in dashed line). The local translational optic flow $\omega_T^{KF}$ (in red) measured with the PPK strategy had a SnR of $25.74dB$ (a.ii) and with the RPK strategy of $25.91dB$ (b.ii). The theoretical local translational optic flow was computed as the ratio between $V_x$ and $h$ (in dashed line). The estimates of the flight height $\hat{h}$ converged quickly (within $4s$) to the ground truth $h$ in both cases (a and b.iii). The average percentage error of $\hat{h}$ with respect to $h$ after convergence was $-2.16\%$ for the PPK strategy (with a range of $[-36.89\%, 34.13\%]$) (a.iv) and $-2.58\%$ for the RPK strategy (with a range of $[-36.89\%, 34.23\%]$) (b.iv). The final percentage error in the estimates of the distance traveled $\hat{X}_{SOFIa}$ with respect to the ground truth $X_{gt}$ was $-1.22\%$ for the PPK strategy (a.v) and $-2.84\%$ for the RPK strategy (b.v).

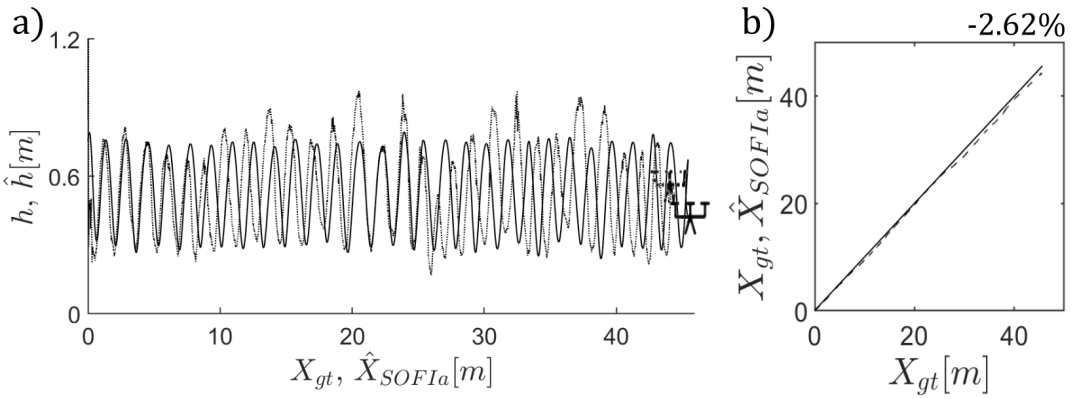


Figure 7: a) Comparison of the position of the hexarotor in the vertical plane ($x$,$z$) estimated with the **R**ough **P**rior **K**nowledge (RPK) fusion strategy (dashed line) to the ground truth given by the MoCap system (continuous line). The estimates of the flight height $\hat{h}$ were plotted on the estimates of the traveled distance $\hat{X}_{SOFIa}$, while the ground truth $h$ was plotted on $X_{gt}$. This test flight was performed at $1518lux$. b) The final percentage error in the estimates of the traveled distance $\hat{X}_{SOFIa}$ with respect to the ground truth $X_{gt}$ was $-2.62\%$.

of the flight height after convergence (considered at $4s$). The flight height error was $-9.77\%$ for the NPK method (see figure 5), while it was $-2.16\%$ for the PPK strategy and $-2.84\%$ for the RPK strategy. Similar results were obtained for all 14 datasets. The SnR of the local translational optic flow measured with the NPK method ranged between $18.08dB$ and $24.79dB$, while with the PPK strategy it ranged between $24.84dB$ and $29.93dB$ and with the RPK strategy it ranged between $24.84dB$ and $28.64dB$. The SnR of the local optic flow divergence measured with the NPK method ranged between $5.41dB$ and $5.71dB$, while with both the PPK and RPK strategies it ranged between $6.47dB$ and $7.1dB$.

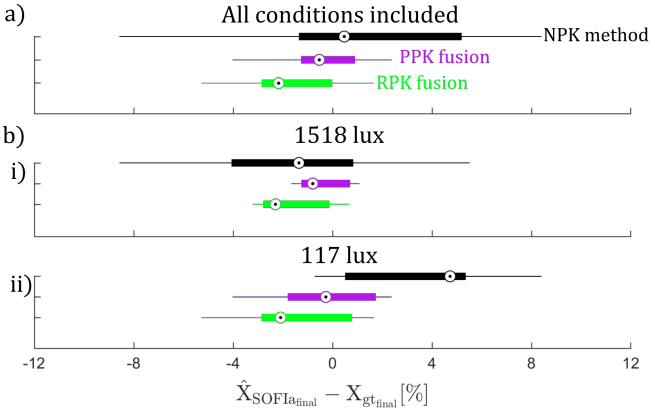


Figure 8: a) When considering all 14 datasets taken, the final percentage error ranged between $-8.57\%$ and $8.4\%$ (with a median of $0.47\%$) for the **N**o **P**rior **K**nowledge (NPK) method (in black), between $-4.02\%$ and $2.38\%$ (with a median of $-0.53\%$) for the **P**recise **P**rior **K**nowledge (PPK) strategy (in purple) and between $-5.27\%$ and $1.66\%$ (with a median of $-2.17\%$) for **R**ough **P**rior **K**nowledge (RPK) (in green). b.i) At $1518lux$, the final percentage error ranged between $-8.57\%$ and $5.52\%$ (with a median of $-1.14\%$) for the NPK method, between $-1.65\%$ and $1.08\%$ (with a median of $-0.8\%$) for the PPK strategy and between $-3.21\%$ and $0.67\%$ (with a median of $-2.3\%$) for RPK strategy. b.ii) At $117lux$, the final percentage error ranged between $-0.72\%$ and $8.4\%$ (with a median of $4.73\%$) for the NPK method, between $-4.02\%$ and $2.38\%$ (with a median of $-0.27\%$) for the PPK strategy and between $-5.27\%\%$ and $1.66\%$ (with a median of $-2.09\%$) for the RPK strategy.

The computation of the estimates of the flight height $\hat{h}$ and of the estimates of the traveled distance $\hat{X}_{SOFIa}$ allow to assess the position of the hexarotor in the vertical plane ($x$,$z$). An example is shown in Figure 7, in which the estimates of the flight height $\hat{h}$ were plotted on the estimates of the traveled distance $\hat{X}_{SOFIa}$ (which are given directly in meters) and compared to the ground truth given by the MoCap system. Since it is based on the optic flow based odometry, the 2D position estimation is subject to an accumulation of error increasing with the distance covered.

Overall, the final percentage error in the estimates of the distance traveled $\hat{X}_{SOFIa}$ with respect to the ground truth $X_{gt}$ (traveled along the $x$ axis) ranged between $-8.57\%$ and $8.4\%$ for the NPK method, between $-4.02\%$ and $2.38\%$ for the PPK strategy and between $-5.27\%$ and $1.66\%$ for the RPK strategy (see Figure 8.a). Similar results were obtained when considering the two different illuminances separately (see Figure 8.b).

## 8 CONCLUSION

In this study, we investigated how to use some knowledge of the oscillating trajectory to improve a minimalistic odometry based on optic flow cues. The experiments were performed onboard a hexarotor following circular bouncing trajectories at a frequency of $0.28Hz$ over distances of about $50m$ under illuminances of $117lux$ and $1518lux$. Results were not influenced by illuminance conditions.

Our findings show that the sensor fusion strategies based on the use of 4 optic flow sensors allowed to measure the optic flow divergence and the translational flow cues more reliably thanks to filtering made by additional Kalman Filters. This was the case even when taking into consideration only a rough prior knowledge of the optic flow variations and more specifically only the oscillation timing of the trajectory. This prior knowledge can be considered acceptable since the oscillation timing is imposed by the drone itself on its own forward trajectory. The sensor fusion strategies decreased the error in the estimates of the flight height. Consequently, they decreased the percentage error in the estimates of the distance traveled in every case considered and thus improved odometry performance.

For all three methods, we acknowledge that the final traveled distance estimates are subject to a small error as the odometry strategy is a dead reckoning method without any feedback from the environment. Such a minimalistic optic flow based odometry strategy would allow a future drone to assess whether it is returning near its base station without GPS. So far, our findings can be considered as a first experimental proof-of-concept of the SOFIa model [23] before implementing such optic flow based odometry strategy on a nanodrone relying on low-computational power, as considered in [26]. Furthermore, we need to validate the robustness of these strategies in a range of forward speeds, in case of large drone pitch, in the presence of reliefs and finally outdoors.

Future work will also include the implementation of an optic flow regulator to keep the translational optic flow around a given setpoint.

## ACKNOWLEDGMENT

We thank J.M. Ingargiola for his help in the design of the printed circuit boards for the optic flow sensors. Financial support was provided via a ProxiLearn project grant to F.R. from the ANR (Astrid Program). The participation of L.B. in this research project was supported by a joint PhD grant from the Délégation Générale de l'Armement (DGA) and Aix Marseille University. L.B, and F.R. were also supported by Aix Marseille University and the CNRS (Life Science, Information Science Institute as well as Engineering Science & Technology Institute). We are grateful to the three anonymous referees, whose suggestions helped us to greatly improved the manuscript.

## REFERENCES

[1] R. Strydom, S. Thurrowgood, and M. V. Srinivasan. Visual odometry: autonomous uav navigation using op-

tic flow and stereo. In Proceedings of Australasian conference on robotics and automation, 2014.

[2] V. More, H. Kumar, S. Kaingade, P. Gaidhani, and N. Gupta. Visual odometry using optic flow for unmanned aerial vehicles. In 2015 International Conference on Cognitive Computing and Information Processing(CCIP), pages 1–6, 2015.

[3] A. R. Vidal, H. Rebecq, T. Horstschaefer, and D. Scaramuzza. Ultimate slam? combining events, images, and imu for robust visual slam in hdr and high-speed scenarios. IEEE Robotics and Automation Letters, 3(2):994–1001, 2018.

[4] A. Denuelle and M. V. Srinivasan. A sparse snapshot-based navigation strategy for uas guidance in natural environments. In 2016 IEEE International Conference on Robotics and Automation (ICRA), pages 3455–3462. IEEE, 2016.

[5] F. Kendoul, I. Fantoni, and K. Nonami. Optic flow-based vision system for autonomous 3d localization and control of small aerial vehicles. Robotics and autonomous systems, 57(6-7):591–602, 2009.

[6] M. Faessler, F. Fontana, C. Forster, E. Mueggler, M. Pizzoli, and D. Scaramuzza. Autonomous, vision-based flight and live dense 3d mapping with a quadrotor micro aerial vehicle. Journal of Field Robotics, 33(4):431–450, 2016.

[7] S. H. Lee and G. de Croon. Stability-based scale estimation for monocular slam. IEEE Robotics and Automation Letters, 3(2):780–787, 2018.

[8] R. Milijas, L. Markovic, A. Ivanovic, F. Petric, and S. Bogdan. A comparison of lidar-based slam systems for control of unmanned aerial vehicles. In 2021 International Conference on Unmanned Aircraft Systems (ICUAS), pages 1148–1154. IEEE, 2021.

[9] A. Shurin and I. Klein. Qdr: A quadrotor dead reckoning framework. IEEE Access, 8:204433–204440, 2020.

[10] F. Ruffier and N. Franceschini. Optic flow regulation: the key to aircraft automatic guidance. Robotics and Autonomous Systems, 50(4):177–194, 2005.

[11] F. Expert and F. Ruffier. Flying over uneven moving terrain based on optic-flow cues without any need for reference frames or accelerometers. Bioinspiration and Biomimetics, 10, 2015.

[12] F. Iida. Biologically inspired visual odometer for navigation of a flying robot. Robotics and autonomous systems, 44(3-4):201–208, 2003.

[13] F. Kendoul, I. Fantoni, and K. Nonami. Optic flow-based vision system for autonomous 3d localization and control of small aerial vehicles. Robotics and autonomous systems, 57(6-7):591–602, 2009.

[14] J. R Serres and F. Ruffier. Optic flow-based collision-free strategies: From insects to robots. Arthropod structure & development, 46(5):703–717, 2017.

[15] WH Kirchner and MV Srinivasan. Freely flying honeybees use image motion to estimate object distance. Naturwissenschaften, 76(6):281–282, 1989.

[16] G. Portelli, F. Ruffier, F. L. Roubieu, and N. Franceschini. Honeybees' speed depends on dorsal as well as lateral, ventral and frontal optic flows. PloS one, 6(5):e19486, 2011.

[17] B. Herissé, T. Hamel, R. Mahony, and F.-X. Russotto. Landing a vtol unmanned aerial vehicle on a moving platform using optical flow. IEEE Transactions on robotics, 28(1):77–89, 2011.

[18] F. Van Breugel, K. Morgansen, and M. H Dickinson. Monocular distance estimation from optic flow during active landing maneuvers. Bioinspiration & biomimetics, 9(2):025002, 2014.

[19] G. CHE de Croon. Monocular distance estimation with optical flow maneuvers and efference copies: a stability-based strategy. Bioinspiration & biomimetics, 11(1):016004, 2016.

[20] H. W. Ho, G. CHE de Croon, and Q. Chu. Distance and velocity estimation using optical flow from a monocular camera. International Journal of Micro Air Vehicles, 9(3):198–208, 2017.

[21] V. Creuze. Monocular odometry for underwater vehicles with online estimation of the scale factor. In IFAC 2017 World Congress, 2017.

[22] L. Bergantin, T. Raharijaona, and F. Ruffier. Estimation of the distance from a surface based on local optic flow divergence. In 2021 International Conference on Unmanned Aircraft Systems (ICUAS), pages 1291–1298. IEEE, 2021.

[23] L. Bergantin, N. Harbaoui, T. Raharijaona, and F. Ruffier. Oscillations make a self-scaled model for honeybees' visual odometer reliable regardless of flight trajectory. Journal of the Royal Society Interface, 18(182):20210567, 2021.

[24] J. J. Gibson. The perception of the visual world. 1950.

[25] L. Meier, D. Honegger, and M. Pollefeys. Px4: A node-based multithreaded open source robotics framework for deeply embedded platforms. In 2015 IEEE

International Conference on Robotics and Automation (ICRA), pages 6235–6240, 2015.

[26] D. Palossi, A. Marongiu, and L. Benini. Ultra low-power visual odometry for nano-scale unmanned aerial vehicles. In Design, Automation Test in Europe Conference Exhibition (DATE), 2017, pages 1647–1650, 2017.

## APPENDIX A: KALMAN FILTER CALCULATIONS

For the PPK strategy, the optic flow divergence and translational optic flow cues were expressed as in equations (7) and (8), respectively. For the RPK strategy, the optic flow divergence and translational optic flow cues were both expressed as in equation (9). For each optic flow cue, at each $k^{th}$ step the current value of the corresponding model was computed and given to the corresponding KF as input (see Figure 3). In the following paragraph, the notation $A > 0$ indicates a matrix strictly positive definite. The KF took the following iterative steps for each $k^{th}$ time:

**Prediction step**

(a) One-step ahead prediction

$$X_{k/k-1} = \Phi \cdot X_{k-1/k-1} + \Gamma \cdot U_{k-1/k-1} \tag{11}$$

with $\Phi > 0, \Gamma > 0$.

(b) Covariance matrix of the state prediction error vector

$$P_{k/k-1} = \Phi \cdot P_{k-1/k-1} \cdot \Phi^T + Q \tag{12}$$

**Correction step**

(c) Measurement update

$$X_{k/k} = X_{k/k-1} + K_k \cdot (Y_k^i - H_k \cdot X_{k/k-1}) \tag{13}$$

with $Y_k^i$ current value of the $i^{th}$ measurement, $H_k > 0$ and $K_k$ Kalman gain defined as:

$$K_k = P_{k/k-1} \cdot H_k^T \cdot [H_k \cdot P_{k/k-1} \cdot H_k^T + R_k]^{-1} \tag{14}$$

The measurement update step was repeated for each $i^{th}$ measurement (2 times for the optic flow divergence and 3 times for the translational optic flow).

(d) Covariance matrix of state estimation error vector

$$P_{k/k} = P_{k/k-1} + K_k \cdot [H_k \cdot P_{k/k-1} \cdot H_k^T + R_k] \cdot K_k^T \tag{15}$$

(e) Innovation

$$\tilde{Y_k} = Y_k - H_k \cdot X_{k/k} \tag{16}$$

## APPENDIX B: EXTENDED KALMAN FILTER CALCULATIONS

The discretized model of the hexarotor (equation (6)) can be expressed as

$$\begin{cases} X[k+1] = \Phi \cdot X[k] + \Gamma \cdot U[k] \\ Y[k] = C_k \cdot X[k] + D_k \cdot U[k] \end{cases} \tag{17}$$

with

$$\Phi = e^{A \cdot dt} \tag{18}$$

$$\Gamma = (\int_0^{dt} e^{A \cdot \tau} d\tau) \cdot B = (A^T \cdot e^{A \cdot dt} - A^T) \cdot B \tag{19}$$

$$C_k = h(X_k) = \begin{bmatrix} \frac{X_2[k]}{X_1[k]} \end{bmatrix} \tag{20}$$

$$D_k = 0 \tag{21}$$

where $dt$ is the discretization time. To estimate the flight height $h$, the EKF took the following iterative steps for each $k^{th}$ time:

**Prediction step**

(a) One-step ahead prediction

$$X_{k/k-1} = \Phi \cdot X_{k-1/k-1} + \Gamma \cdot U_{k-1/k-1} \tag{22}$$

(b) Covariance matrix of the state prediction error vector

$$P_{k/k-1} = \Phi \cdot P_{k-1/k-1} \cdot \Phi^T + Q \tag{23}$$

**Correction step**

(c) Measurement update

$$X_{k/k} = X_{k/k-1} + K_k \cdot (Y_k - H_k \cdot X_{k/k-1}) \tag{24}$$

with $K_k$ Kalman gain defined as:

$$K_k = P_{k/k-1} \cdot H_k^T \cdot [H_k \cdot P_{k/k-1} \cdot H_k^T + R_k]^{-1} \tag{25}$$

and $H_k$ Jacobian matrix for the non linear function defined as follows:

$$H_k = \frac{\partial h}{\partial X}|_{X=X_{k/k-1}} = \begin{bmatrix} -\frac{\dot{h}}{h^2} & \frac{1}{h} \end{bmatrix} \tag{26}$$

(d) Covariance matrix of state estimation error vector

$$P_{k/k} = P_{k/k-1} + K_k \cdot [H_k \cdot P_{k/k-1} \cdot H_k^T + R_k] \cdot K_k^T \tag{27}$$

(e) Innovation

$$\tilde{Y_k} = Y_k - H_k \cdot X_{k/k} \tag{28}$$